Proceedings of PVP2003
2003 ASME Pressure Vessels and Piping Conference
July 20-24, 2003 Cleveland Ohio, USA

PVP2003-1982

EVALUATION OF FRACTURE TOUGHNESS FROM INSTRUMENTED CHARPY IMPACT TESTS FOR A REACTOR PRESSURE VESSEL STEEL.

A. PARROT
EDF R&D, Materials and Mechanics of Components department, Avenue des Renardières - Ecuelles, F-77818 Moret-Sur-Loing Cedex
France

P. FORGET
CEA/CEREM/SRMA
F-91191 Gif-Sur-Yvette
France

A. DAHL
EDF R&D, Materials and Mechanics of Components department, Avenue des Renardières - Ecuelles, F-77818 Moret-Sur-Loing Cedex
France

ABSTRACT

The monitoring of neutron induced embrittlement of nuclear power plants is provided using Charpy impact test in the surveillance program. However structural integrity assessments require the fracture toughness. Some empirical formulas have been developed but no direct relationship was found. The aim of our study is to determine the fracture toughness of a Reactor Pressure Vessel steel from instrumented Charpy impact test using local approach to fracture. This non-empirical method has been applied in the brittle domain as well as in the ductile to brittle transition for an A508 Cl.3 steel. In the brittle domain, fracture occurs by cleavage and can be modeled with the Beremin model. Fracture toughness has been successfully determined from Charpy impact tests results and the influence of several parameters (mesh design, Beremin model with one or two parameters, number of Charpy impact tests results) on the results was considered. In the ductile to brittle transition, cleavage fracture is preceded by ductile crack growth. Ductile tearing has been accounted for in the simulations with the Rousselier model whereas cleavage fracture is still described with the Beremin model. The determination of fracture toughness from Charpy impact tests gave encouraging results but finite element simulations have to be refined in order to improve predictions.

INTRODUCTION

The monitoring of neutron induced embrittlement of nuclear power plants is provided using Charpy impact test in the surveillance program. However structural integrity assessments require the fracture toughness. Some empirical formulas have been developed but no direct relationship was found. The aim of our study is to determine the fracture toughness of a Reactor Pressure Vessel steel from instrumented Charpy impact test using local approach to fracture.

The method can be divided in three main steps [1]. The first step is the finite element simulation of Charpy impact tests in order to determine the local mechanical fields used in the local approach. The second step is the identification of a rupture model through the comparison of the simulations with Charpy experimental results. Finally, a finite element simulation of fracture toughness is performed and the failure statistic is determined with the previously identified rupture model.

This non-empirical method will be applied in the brittle domain as well as in the ductile to brittle transition for an A508 Cl.3 steel. In the brittle domain, fracture occurs by cleavage and can be modeled with the Beremin model. The fracture toughness prediction from Charpy impact tests will be performed at one temperature in the brittle domain and the influence of the mesh design and of the choice of the Beremin model parameters will be considered. In the ductile to brittle transition, cleavage fracture is preceded by ductile crack growth. Ductile tearing is accounted for in the simulations with the Rousselier model whereas cleavage fracture is still described with the Beremin model. The fracture toughness prediction from Charpy impact tests will be performed at three different temperatures in the ductile to brittle transition.

All the simulations are performed with Code_Aster finite element code.

EXPERIMENTAL

A French 16MND5 steel (equivalent of the American ASTM Standard A508 Cl.3) extracted from the real nozzle of the shell of a RPV was studied. The chemical composition is given in Table I. The microstructure corresponds to upper bainite. The primary austenite grain size is about 30 µm, the mean size of bainitic packets is about 10 µm. The lath width varies between 1 and 2 µm [2]. The standard CT25 (1T) specimens and Charpy V-Notch (CVN) specimens were sampled in the T-S (long transverse-short transverse) orientation. Fracture toughness K_{IC} was determined according to the norm ASTM E399. For tests exceeding 5% deviation of force direction, either fracture toughness K_{cpm} was determined according to RCC-M code [3] (annex ZG) or fracture toughness K_{JC} was determined from the J-integral given by the norm ASTM E 813. The tests were carried out at various temperatures ranging from -196°C to room temperature. The results presented in Fig. 1 and Fig. 2 correspond to a selection of four different temperatures : -90°C, -60°C, -30°C and 0°C.

C	Mn	Ni	Mo	P	S	Si	Cr
0.16	1.30	0.7	0.51	0.008	0.006	0.20	0.20

Table I. Chemical composition of 16MND5 steel (weight %).

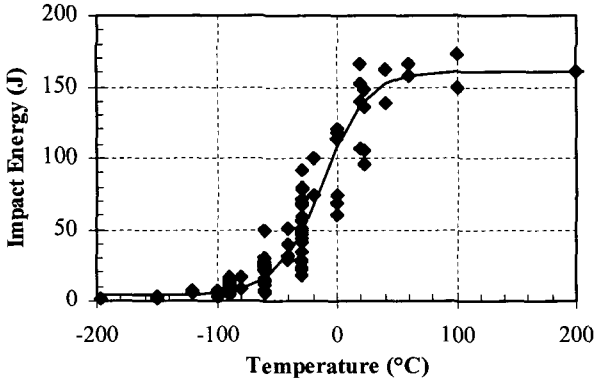

Fig. 1. Results of impact tests on CVN specimens on 16MND5 steel.

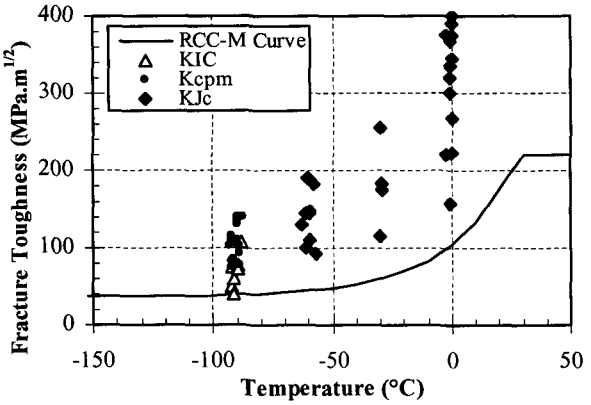

Fig. 2. Results of fracture toughness tests on 16MND5 steel.

At -90°C rupture occurs by cleavage and no ductile tearing can be found whereas from -60°C fractographic studies have shown that ductile tearing occurs before the final rupture by cleavage.

FROM CHARPY IMPACT TEST TO FRACTURE TOUGHNESS IN THE BRITTLE DOMAIN

At low temperatures in the brittle domain, several works on the simulation of Charpy impact test [4, 5] have shown that it can be modeled with a 2D mesh in Plain Strain condition. The viscosity of the material has to be taken into account but the inertial effects due to impact can be neglected.

The transition from Charpy impact test to fracture toughness was performed at -90°C in the brittle domain.

Constitutive equations

For the simulation of CT specimens, the plastic hardening behavior is given as a table (see Table VI in Appendix).

For the simulation of Charpy tests, the material behavior is simulated with a Lemaître law in order to take into account viscous effects due to high strain rates :

$$\sigma = K\varepsilon^{1/M}\left(d\varepsilon/dt\right)^{1/N}$$

where K, N and M are parameters, $K = 1207.9$, $N = 48.6145$ and $M = 9.0934$ at -90°C. The parameters of the Lemaître law were identified from compressive tests performed on a Hopkinson bar device (strain rate $1000s^{-1}$) and on an hydraulic testing machine (strain rate $1s^{-1}$ and $4.10^{-3}s^{-1}$).

Numerical modeling

Charpy tests were modeled in a 2D Plain strain or 3D formulation. In 2D, different mesh sizes at the notch root were used from (25x25)µm² to (100x100)µm². In 3D the mesh size at the notch root is (50x125)µm² in section. Due to symmetry considerations, only one half (2D) or one quarter (3D) of the specimen needs to be modeled. Quadratic elements with reduced integration were employed. The computations were performed in the framework of finite strains with an updated-Lagrangian formulation. The experimental and simulated load versus striker's displacement diagram are shown in Fig. 3. A good agreement is obtained between experimental results and the simulations. The 2D simulations give the same results for all the mesh sizes. The 3D simulation reproduces better the experimental load level.

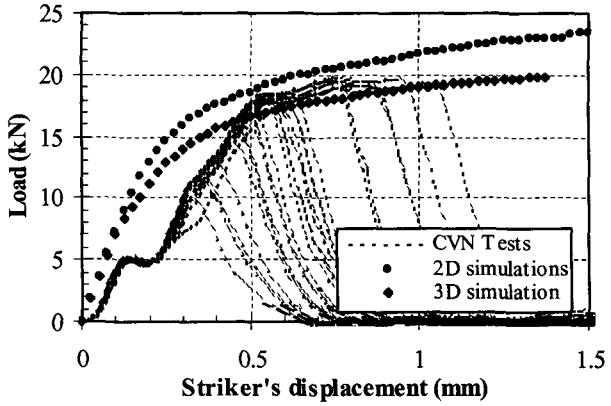

Fig. 3. Experimental and simulated load versus striker's displacement diagram for Charpy tests at -90°C.

Cleavage fracture is described using the Beremin model [6]. In this model based on the weakest-link theory, the failure probability is given by :

$$P_r = 1 - \exp\left[-\left(\frac{\sigma_w}{\sigma_u}\right)^m\right]$$ where m and σ_u are the parameters and σ_w is the Weibull stress defined by :

$$\sigma_w = \left(\int_{V_p} \sigma_I^m \frac{dV}{V_0}\right)^{\frac{1}{m}}$$ where σ_I is the positive maximum principal stress and V_p is the plastic volume.

The plastic zone is defined above 10^{-6} of equivalent plastic strain and $V_0 = (50\mu m)^3$ was employed.

A numerical study conducted on the Beremin model has shown that the two parameters m and σ_u are not independent [1]. For the identification of (m, σ_u) from a set of fracture results, m can be fixed and only σ_u has to be optimized in order to fit the results. Four identifications of the Beremin model were performed : three with an imposed value of m (20, 24 and 28 which are classical values for an A508 Cl.3 steel) and one with both m and σ_u free to vary. These identifications are made using a post-treatment of the finite element results for the Charpy impact test, details about the identification method can be found in [1, 7]. The results of the identifications are shown in Table II.

Mesh size at the notch root		m fixed $m = 20$	m fixed $m = 24$	m fixed $m = 28$	m and σ_u free to vary
(25x25)µm²	m	20	24	28	38
2D	σ_u	3168	2890	2710	2466
(50x50)µm²	m	20	24	28	37
2D	σ_u	3162	2884	2705	2472
(100x100)µm²	m	20	24	28	38
2D	σ_u	3145	2868	2689	2437
(50x125)µm²	m	20	24	28	35
3D	σ_u	3158	2904	2713	2533

Table II. Identification of the Beremin model on Charpy impact tests at -90°C.

For each identification, the parameters set (m, σ_u) varies little with the mesh size. Fig. 4 shows the results of the identification for the 2D (50x50)µm² mesh. A better agreement with experimental results is obtained when m and σ_u are free to vary.

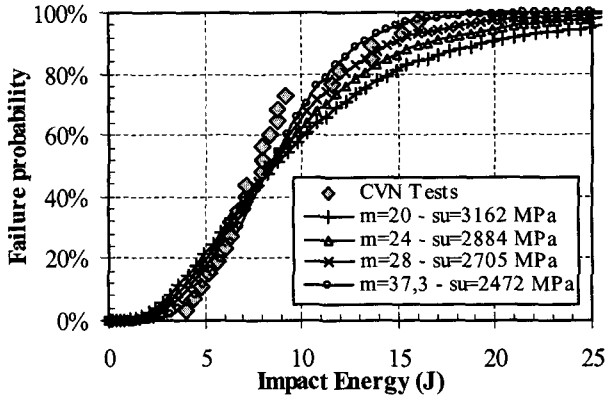

Fig. 4. Failure probability for Charpy tests : comparison between experimental results and the 2D (50x50)µm² simulation.

CT specimens were then modeled in a 2D Plain strain or 3D formulation. Different mesh sizes at the crack tip were used from (25x25)µm² to (100x100)µm² in 2D and from (50x50)µm² to (500x500)µm² in 3D. Due to symmetry considerations, only one half (2D) or one quarter (3D) of the specimen needs to be modeled. Quadratic elements with reduced integration were employed. The computations were performed in the framework of finite strains with an updated-Lagrangian formulation. The fracture toughness is estimated from the elastic energy release rate computed by the theta method in Code_Aster finite element code.

The experimental and simulated load versus Crack Mouth Opening Displacement (CMOD) are shown in Fig. 5. A good agreement is obtained between experimental results and the simulations. The mesh size at the crack tip has no influence on the global results for the 2D and 3D simulations. The 3D simulations reproduce better the experimental load level.

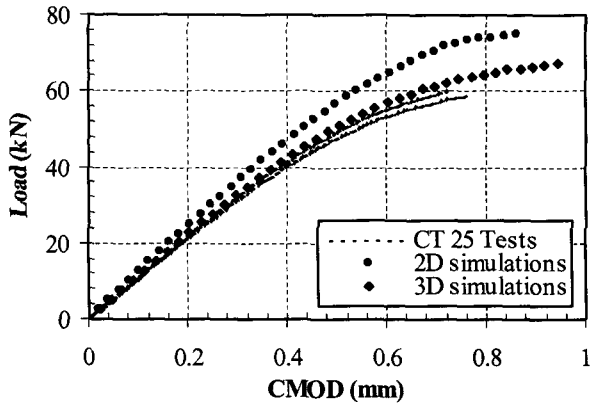

Fig. 5. Experimental and simulated load versus CMOD diagram for CT specimen tests at -90°C.

The opening stress at the crack tip was examined. The chosen mesh sizes at the crack tip have an influence on the calculated opening stress. Moreover, in 3D simulations the mesh refinement in the specimen thickness is not fine enough on the specimen side and leads to an overestimation of the opening stress on the specimen sides. The Beremin model being very sensitive to the stress field in the specimen, this overestimation of the opening stress on the specimen sides will have an influence on the estimated failure probability.

The failure statistics of CT specimens is predicted using the Beremin model identified on Charpy impact tests results.

For 2D simulations, for small values of m (20 or 24), the predicted failure statistic is almost identical for all the mesh designs whereas for higher values of m, some differences appear. The better results are obtained with $m = 20$ and are equivalent for all the meshes but the description of low fracture toughness is not satisfactory.

For 3D simulations, the influence of the mesh size at the crack tip is also revealed. The higher the mesh size at the crack tip is, the less conservative are the results. The better results are obtained with $m = 20$ for the (100x100)µm² mesh, they are shown in Fig. 6 and are in good agreement with experimental results.

We have seen that the best results are obtained with small m values. This could be explain by the fact that the higher m is, the more an error on the estimation of the stress field will influence the Weibull stress and then the failure probability. Furthermore, in order to improve the results, new 3D simulations of CT specimen with a better mesh design on the sides should be done.

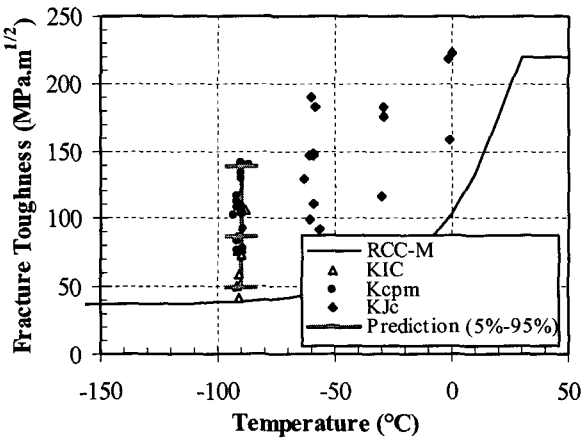

Fig. 6. Fracture toughness prediction (between Pr=5% and Pr=95%) at -90°C with the 3D (100x100)µm² mesh and m=20.

The transition from Charpy impact energy to fracture toughness has been performed here from an initial set of 28 CVN tests. Within the context of the surveillance program a limited number of specimens will be available at each temperature. The influence of the number of CVN tests on the determination of fracture toughness was then studied. The results are presented in details in [7]. If only a small number of Charpy specimens are available, the use of the Beremin model is relevant if the value of m is fixed to an arbitrary value. When determining the value of σ_u, most accuracy is gained by increasing the number of specimens from 3 to about 6. Over 6 specimens, it is necessary to increase highly the number of specimens in order to have a significant gain of accuracy. This study showed that it is feasible to evaluate fracture toughness of an in-service RPV steel from the CVN specimens of the surveillance program in the brittle domain.

FROM CHARPY IMPACT TEST TO FRACTURE TOUGHNESS IN THE DUCTILE TO BRITTLE TRANSITION

In the ductile to brittle transition, ductile crack growth occurs before cleavage and must be accounted for in the simulations. The simulation of Charpy impact test and fracture toughness have to be performed with a 3D formulation in order to have a good description of the ductile crack growth. For Charpy impact test, the viscosity of the material has to be taken into account but the inertial effects due to impact can still be neglected. For simplicity reasons, the temperature rise due to the local high strain rates in Charpy specimens is not taken into account.

The transition from Charpy impact test to fracture toughness was performed at -60°C, -30°C and 0°C in the ductile to brittle transition.

Constitutive equations

Ductile crack growth in the Charpy and CT specimens was numerically modeled using the Rousselier model [8]. The yield condition is given by :

$$\phi = \frac{\sigma_{eq}}{\rho} + D\sigma_1 f \exp\left(\frac{\sigma_m}{\rho\sigma_1}\right) - R(p) = 0$$

where σ_{eq} is the macroscopic Von Mises stress,

σ_m is the hydrostatic stress,

$\rho = \frac{1-f}{1-f_0}$ is the relative density with f and f_0 the present and initial void volume fraction,

σ_1 is the matrix resistance to the cavity growth,

D is a constant of integration,

$R(p)$ is the yield stress of the undamaged material and depends on the equivalent plastic strain.

The parameters are D, σ_1 and f_0. For all the simulations, D is taken as prescribed by [8] : $D = 2$. The initial void volume fraction f_0 was taken as the volume fraction of MnS inclusions given by the Franklin formula [9] : $f_0 = 5.10^{-4}$. The matrix resistance to the cavity growth σ_1 is dependant of the strain-rate. For the CT modeling under quasi-static condition, σ_1 was chosen in order to fulfill the load drop in the load versus reduction of diameter diagram of notched tensile specimens (NT2, NT4 et NT10). For Charpy impact test modeling, σ_1 was chosen in order to fulfill the load drop in the load versus striker's displacement diagram of instrumented Charpy tests. For the three considered temperatures, the parameters are summarized in Table III.

The mesh size is also a parameter for such damage models which lead to a softening of the material. The mesh size at the crack tip or notch root was chosen equal to (200x200)µm² in order to have a reasonably good description of the stress field and acceptable computation durations. This mesh size is higher than the usually recommended mesh sizes for the use of the Beremin model which are of the order of (50x50)µm². Nevertheless in the ductile to brittle transition large plastic

strains occur, the stress field is more averaged and a mesh size of (200x200)μm² is acceptable.

	T	σ_1	D	f_0
Charpy impact test modeling	-60°C	715 MPa	2	5.10^{-4}
	-30°C	620 MPa		
	0°C	575 MPa		
CT modeling	-60°C	520 MPa	2	5.10^{-4}
	-30°C	490 MPa		
	0°C	480 MPa		

Table III. Parameters used for ductile crack growth modeling.

For the simulation of CT specimens, the plastic hardening behavior $R(p) = \sigma_{y-qstat}(p)$ is given as a table (see Table VII in Appendix).

For the simulation of Charpy impact tests viscous effects must be accounted for, the plastic behavior is described by :

$$R(p,\dot{p}) = \sigma_{y-visc}(p) + \sigma_0 sh^{-1}\left[\left(\frac{\dot{p}}{\dot{\varepsilon}_0}\right)^{\frac{1}{q}}\right] \quad \text{where} \quad \sigma_{y-visc}(p)$$

is given as a table (see Table VIII in Appendix) and σ_0, $\dot{\varepsilon}_0$ and q are parameters which are given in Table IV. These parameters were identified from compressive tests performed on a Hopkinson bar device (strain rate between $20s^{-1}$ and $2600s^{-1}$) on a second A508 Cl.3 steel extracted from the shell of a RPV.

T	σ_0	q	$\dot{\varepsilon}_0$
-60°C	94830	9.1157	2.223839 E27
-30°C	75593	7.7464	1.734382 E23
0°C	61763	6.7619	1.931237 E20

Table IV. Parameters used in order to take into account viscous effects.

Numerical modeling

Charpy tests were modeled in a 2D Plain strain or 3D formulation. In 2D and 3D, the mesh size at the notch root is (200x200)μm². Quadratic elements with reduced integration were employed. Due to symmetry considerations, only one half (2D) or one quarter (3D) of the specimen needs to be modeled. The computations were performed in the framework of finite strains with an updated-Lagrangian formulation. At the three temperatures (-60°C, -30C° and 0°C), the 3D simulations are in good agreement with experimental results. 2D simulations lead to an overestimation of the load level and of the ductile crack growth kinetic. An example of the experimental and simulated load versus striker's displacement diagram at 0°C is shown in Fig. 7.

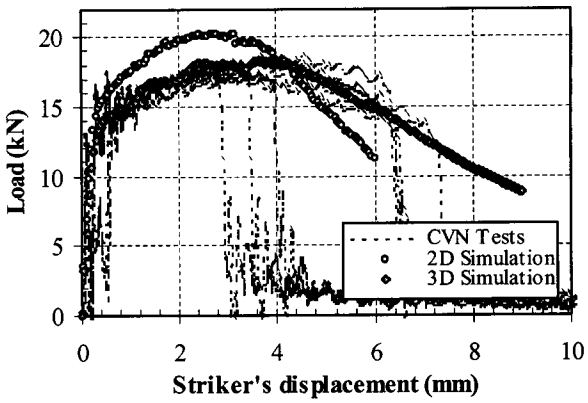

Fig. 7. Experimental and simulated load versus striker's displacement diagram for Charpy tests at 0°C.

The evolution of void volume fraction in the simulated CVN specimens has been studied. The ductile tearing propagation is more important at the center of the specimens than on the sides : the tunneling effect observed experimentally is qualitatively reproduced. At 0°C after a few millimeters propagation, the ductile tearing turns off and is no longer in the symmetry plan. Due to the symmetry conditions imposed for the computation, the branching of ductile tearing leads to simulate the propagation of two cracks. Then the energy needed to propagate the crack is overestimated by this simulation. At -60°C and -30°C, the ductile crack growth is less important and no branching has been observed.

Cleavage fracture is described using the Beremin model. In the ductile to brittle transition, important plastic strain occurs before the rupture by cleavage. The influence of plastic strain on cleavage was taken into account in the Beremin model by modifying the Weibull stress as proposed by Beremin [6] :

$$\sigma_w = \left(\int_{V_p} \sigma_I^m \exp\left(-\frac{m\varepsilon_I^p}{2}\right)\frac{dV}{V_0}\right)^{\frac{1}{m}} \quad \text{where} \quad \varepsilon_I^p \text{ is the}$$

plastic strain in the direction of the maximum principal stress. The Beremin model was also used without the plastic strain correction but the predicted fracture toughness were then largely overestimated.

Three identifications of the Beremin model with an imposed value of m (20, 24 and 28) were performed with the 3D simulations. The results of the identifications are shown in Table V. The critical cleavage stress σ_u increases with temperature. Fig. 8 shows an example of the results of the identification at -30°C.

Temperature		m fixed $m = 20$	m fixed $m = 24$	m fixed $m = 28$
-60°C	σ_u	2906	2650	2487
-30°C	σ_u	2968	2706	2538
0°C	σ_u	3391	3067	2858

Table V. Identification of the Beremin model on Charpy impact tests at -60°C, -30°C and 0°C.

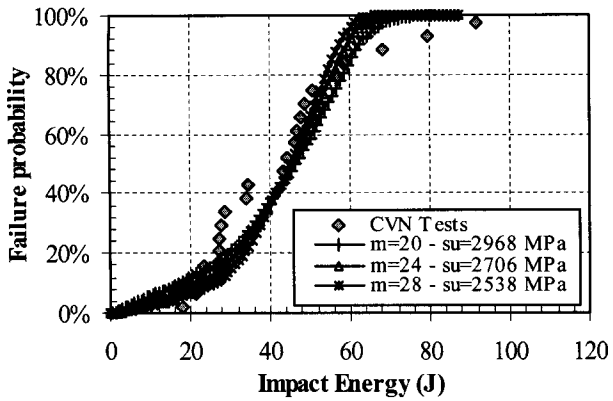

Fig. 8. Failure probability for Charpy tests : comparison between experimental results and the 3D simulation at -30°C.

CT specimens were modeled in a 2D Plain strain or 3D formulation. In 2D and 3D the mesh size at the crack tip is (200x200)μm². For these simulations, the mesh size in the specimen thickness decreases from the center to the sides of the specimen. Due to symmetry considerations, only one half (2D) or one quarter (3D) of the specimen needs to be modeled. Quadratic elements with reduced integration were employed. The computations were performed in the framework of finite strains with an updated-Lagrangian formulation. The fracture toughness is evaluated from the J-Integral computed from the area under the load versus CMOD diagram.

Numerical record of the load versus CMOD diagram is only available at -60°C, it is compared with the simulations in Fig. 9. The 3D simulation is in good agreement with experimental results whereas the 2D simulation overestimates the load level.

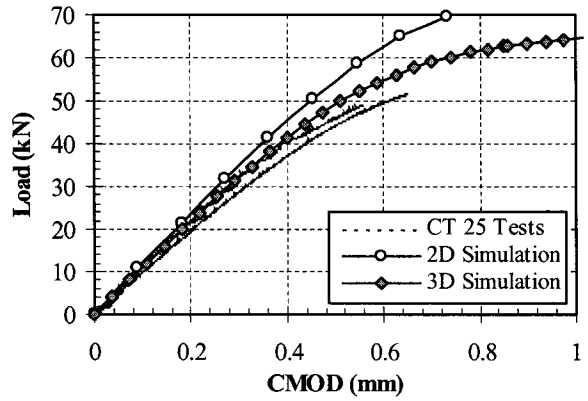

Fig. 9. Experimental and simulated load versus CMOD diagram for CT specimen at -60°C.

The evolution of void volume fraction in the simulated CT specimens has been studied. As for the CVN specimens, the ductile tearing propagation is more important at the center of the specimens than on the sides. At 0°C, the ductile tearing turns off and is no longer in the symmetry plan again, the energy needed to propagate the crack is overestimated by this simulation.

The failure statistics is predicted using the Beremin model identified on Charpy impact tests results.

For all the chosen m (20, 24 and 28) values, the simulated failure statistics are similar. Nevertheless the higher m is, the less conservative are the results. The best results are obtained again with $m = 20$. The fracture toughness prediction with $m = 20$ at -60°C, -30°C and 0°C is shown in Fig. 10. At -60°C and -30°C the simulated failure statistic agrees well with experimental results. The methodology employed allowed to simulate the rise of the lower bound of fracture toughness and of the scattering observed experimentally in the ductile to brittle transition.

At 0°C, the lower bound of fracture toughness is well predicted but the upper bound is underestimated. This could be explained first by the fact that this prediction is based on false simulations. Indeed we have seen that for the Charpy specimen as well as for the CT specimen, the simulated ductile tearing turns off the symmetry plane after a few millimeters propagation. Next, the applicability of the Beremin model after large plastic strains and ductile tearing is questionable. Especially it has been recently emphasized [2] that the fracture mechanisms i.e. defects population evolve with temperature in the ductile to brittle transition. Fractographic studies are necessary in order to clarify fracture mechanisms in the ductile to brittle transition.

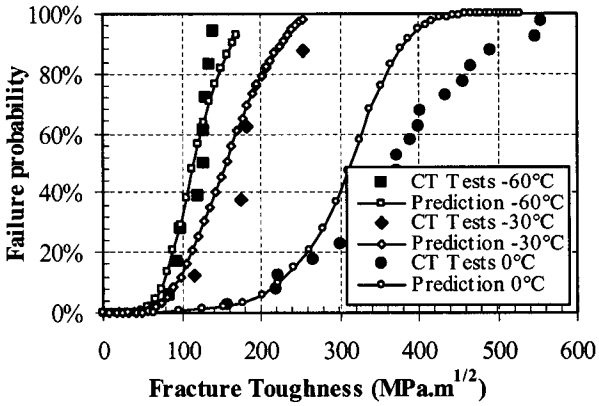

Fig. 10. Fracture toughness prediction at -60°C, -30°C and 0°C with m=20.

The fracture toughness prediction obtained by using the exposed methodology at -90°C, -60°C and -30°C is reminded in Fig. 11.

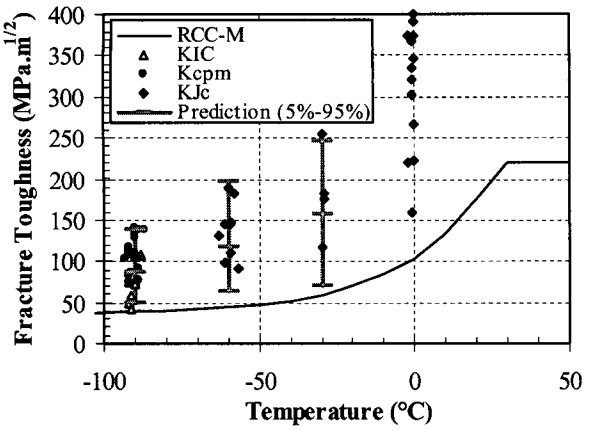

Fig. 11. Fracture toughness prediction (between Pr=5% and Pr=95%) at -90°C, -60°C and -30°C with m=20.

CONCLUSION

In the brittle domain, fracture toughness can be deduced from Charpy impact tests with local approach to fracture. A 2D plane strain simulation of Charpy impact test with a mesh size at the notch root equal to (100x100)µm² is sufficient to identify the Beremin model. A 3D simulation of a CT specimen with a mesh size at the notch tip equal to (100x100)µm² followed by the application of the Beremin model identified with *m* fixed to 20 allows to have a good prediction of the failure statistic.

In the ductile to brittle transition, ductile tearing was modeled with the Rousselier model and the Beremin model was modified in order to take into account the influence of large plastic strains on cleavage triggering. In the lower part of the ductile to brittle transition, the applied methodology with 3D simulations of Charpy impact tests and of CT specimens allowed to simulate the rise of the lower bound of fracture toughness and of the scattering observed experimentally. At higher temperatures, the numerical branching of ductile crack growth must be eliminated by simulating the upper and lower halves of the CT specimens. Moreover, fractographic studies are still necessary in order to identify fracture mechanisms and to verify the validity of the Beremin model.

REFERENCES

[1] N. Verdière, A. Parrot, P. Forget, J.M. Frund « Fracture toughness determination of a nuclear pressure vessel steel by instrumented Charpy impact test », 2001, 9th International Conference on Nuclear Engineering, ICONE 9, Nice, France.

[2] P. Hausild, P. Bompard, C. Berdin, C. Prioul, M. Karlik « Influence of ductile tearing on cleavage triggering in ductile-to brittle transition of A508 steel », 2002 in "From Charpy to Present Impact Testing" D. François and A. Pineau (Eds.), Elsevier Science Ltd. and ESIS.

[3] RCC-M « Résistance à la rupture brutale » Annexe ZG, 1985.

[4] A. Rossol « Détermination de la ténacité d'un acier faiblement allié à partir de l'essai Charpy Instrumenté », 1999, Ph.D. Thesis, Ecole Centrale Paris, France.

[5] M. Tahar « Applications de l'approche locale de la rupture fragile à l'acier 16MND5 : Corrélation résilience-ténacité, probabilité de rupture bi-modale (clivage et intergranulaire) », 1998, Ph.D. Thesis, Ecole des Mines de Paris.

[6] F.M. Beremin « A local criterion for cleavage fracture of a nuclear pressure vessel steel », 1983, Metallurgical transactions A, Volume 14A.

[7] P. Forget, B. Marini, N. Verdière « Prediction of brittle fracture toughness value of a RPV steel from the analysis of a limited set of Charpy results », 2001, 9th International Conference on Nuclear Engineering, ICONE 9, Nice, France.

[8] G. Rousselier « Ductile fracture models and their potential in local approach of fracture », 1987, Nuclear Engineering and Design, 105 : 97-111.

[9] A.G. Franklin « Comparison between a quantitative microscope and chemical methods for assessment of non-metallic inclusions », 1969, Journal of the Iron and Steel Institute, Feb. 181-186.

APPENDIX

p	total strain	$R(p)$
0.00E+00	2.66E-03	571
9.82E-03	1.27E-02	609
1.96E-02	2.27E-02	648
2.95E-02	3.27E-02	686
3.93E-02	4.27E-02	715
4.92E-02	5.27E-02	746
5.91E-02	6.27E-02	775
6.89E-02	7.27E-02	797
7.89E-02	8.27E-02	814
8.88E-02	9.27E-02	832
9.87E-02	1.03E-01	844
1.09E-01	1.13E-01	856
1.19E-01	1.23E-01	867
1.39E-01	1.43E-01	887
1.58E-01	1.63E-01	904
1.78E-01	1.83E-01	920
1.98E-01	2.03E-01	934
2.48E-01	2.53E-01	964
2.98E-01	3.03E-01	990
3.48E-01	3.53E-01	1013
3.98E-01	4.03E-01	1033
4.48E-01	4.53E-01	1050
4.98E-01	5.03E-01	1067
5.98E-01	6.03E-01	1095
6.97E-01	7.03E-01	1120
7.97E-01	8.03E-01	1142
8.97E-01	9.03E-01	1161
9.97E-01	1.00265581	1179
1.10E+00	1.10265584	1196
1.20E+00	1.20265586	1211
1.30E+00	1.30265577	1225
1.40E+00	1.40265579	1238
1.50E+00	1.50265581	1251

Table VI. Plastic hardening behavior at –90°C for the CT specimens simulation.

-60°C			-30°C			0°C		
p	total strain	$\sigma_{y-qstat}(p)$	p	total strain	$\sigma_{y-qstat}(p)$	p	total strain	$\sigma_{y-qstat}$
0	0.00262	543.34	0	0.00253	524.15	0.00000	0.0025	495
0.01	0.01281	581.52	0.01	0.01271	561.39	0.00732	0.01	530
0.02	0.02299	619.71	0.02	0.02289	598.64	0.01712	0.02	570
0.03	0.03317	656.01	0.03	0.03307	636	0.02695	0.03	604
0.04	0.04332	687.01	0.04	0.04323	668	0.03680	0.04	634
0.05	0.05344	713.01	0.05	0.05336	694.5	0.04667	0.05	660
0.06	0.06355	735	0.06	0.06346	716.5	0.05656	0.06	681
0.07	0.07366	757.03	0.07	0.07355	734.5	0.06646	0.07	700
0.08	0.08373	772.84	0.08	0.08362	750	0.07638	0.08	716
0.09	0.09380	787.05	0.09	0.09368	762.7	0.08631	0.09	730
0.1	0.10386	799.99	0.1	0.10374	774.13	0.09626	0.1	740
0.11	0.11392	811.88	0.11	0.11379	784.61	0.10622	0.11	749
0.12	0.12398	822.89	0.12	0.12384	794.3	0.11619	0.12	755
0.14	0.14407	842.76	0.14	0.14392	811.76	0.12614	0.13	765
0.16	0.16416	860.36	0.16	0.16400	827.2	0.13311	0.137	770
0.18	0.18423	876.18	0.18	0.18406	841.07	0.13611	0.14	771
0.2	0.20430	890.59	0.2	0.20412	853.66	0.14607	0.15	778
0.25	0.25445	921.88	0.25	0.25426	880.97	0.19591	0.2	809
0.3	0.30458	948.27	0.3	0.30437	903.93	0.29568	0.3	855
0.35	0.35469	971.16	0.35	0.35446	923.8	0.39551	0.4	889
0.4	0.40479	991.44	0.4	0.40455	941.37	0.49537	0.5	917
0.45	0.45488	1009.68	0.45	0.45462	957.15	0.59525	0.6	940
0.5	0.50496	1026.28	0.5	0.50469	971.48	0.69515	0.7	960
0.6	0.60510	1055.65	0.6	0.60482	996.8	0.79507	0.8	977
0.7	0.70522	1081.14	0.7	0.70492	1018.72	0.89498	0.9	993
0.8	0.80533	1103.72	0.8	0.80501	1038.1	0.99491	1	1008
0.9	0.90543	1124.02	0.9	0.90510	1055.49			
1	1.00552	1142.5	1	1.00518	1071.3			

Table VII. Plastic hardening behavior at -60°C, -30°C and 0°C for the CT specimens simulation.

-60°C			-30°C			0°C		
p	total strain	$\sigma_{y-visc}(p)$	p	total strain	$\sigma_{y-visc}(p)$	p	total strain	$\sigma_{y-visc}(p)$
0	0.00256	529.13	0	0.00241	498.87	0	0.00241	477.13
0.0075	0.01021	560.63	0.0075	0.01007	532.68	0.0075	0.01009	512.55
0.0175	0.02038	596.60	0.0175	0.02025	570.04	0.0175	0.02028	550.48
0.0275	0.03053	626.88	0.0275	0.03040	600.45	0.0275	0.03043	580.36
0.0375	0.04065	652.59	0.0375	0.04052	625.49	0.0375	0.04055	604.26
0.0475	0.05076	674.60	0.0475	0.05062	646.38	0.0475	0.05065	623.75
0.0575	0.06085	693.63	0.0575	0.06071	664.04	0.0575	0.06073	639.95
0.0675	0.07093	710.23	0.0675	0.07078	679.20	0.0675	0.07080	653.71
0.0775	0.08100	724.87	0.0775	0.08085	692.42	0.0775	0.08086	665.63
0.0875	0.09106	737.90	0.0875	0.09090	704.11	0.0875	0.09092	676.17
0.0975	0.10112	749.64	0.0975	0.10095	714.60	0.0975	0.10096	685.67
0.1075	0.11117	760.30	0.1075	0.11100	724.15	0.1075	0.11101	694.37
0.1175	0.12122	770.08	0.1175	0.12104	732.95	0.1175	0.12105	702.45
0.1275	0.13126	779.14	0.1275	0.13108	741.14	0.1275	0.13109	710.05
0.1345	0.13829	785.12	0.1345	0.13811	746.58	0.1345	0.13811	715.14
0.1375	0.14130	787.60	0.1375	0.14112	748.85	0.1375	0.14112	717.27
0.1475	0.15134	795.55	0.1475	0.15115	756.16	0.1475	0.15116	724.18
0.1975	0.20151	830.06	0.1975	0.20131	788.66	0.1975	0.20132	755.57
0.2975	0.30178	885.08	0.2975	0.30157	842.55	0.2975	0.30159	808.99
0.3975	0.40199	930.00	0.3975	0.40179	887.32	0.3975	0.40181	853.72
0.4975	0.50217	967.67	0.4975	0.50197	924.97	0.4975	0.50200	891.36
0.5975	0.60233	999.37	0.5975	0.60212	956.67	0.5975	0.60216	923.06
0.6975	0.70246	1026.06	0.6975	0.70225	983.36	0.6975	0.70230	949.75
0.7975	0.80257	1048.53	0.7975	0.80236	1005.83	0.7975	0.80241	972.22
0.8975	0.90266	1067.45	0.8975	0.90245	1024.75	0.8975	0.90251	991.14
0.9975	1.00273	1083.38	0.9975	1.00253	1040.68	0.9975	1.00259	1007.07

Table VIII. Plastic hardening behavior at -60°C, -30°C and 0°C for the CVN specimens simulation.